Theses and Dissertations

5-1-2018

Ultra High Speed Space Division Multiplexing OCT

Guo-Jhe Syu
Lehigh University, s0987599709@gmail.com

Follow this and additional works at: https://preserve.lehigh.edu/etd

Part of the Electrical and Computer Engineering Commons

Ultra high speed Space Division Multiplexing OCT

By

GUO-JHE SYU

A Thesis

Presented to the Graduate and Research Committee

of Lehigh University

in Candidacy for the Degree of

Master of Science

in

Electrical Engineering

Lehigh University

May, 2018

Copyright

By

Guo-Jhe Syu

May 2018

(Guo-Jhe Syu) THESIS SIGNATURE SHEET

This thesis is accepted and approved in partial fulfillment of the requirements for the Master of Science.

Date

_____

Thesis Advisor

_____

Department Chair

Acknowledgement

First, A huge amount of gratitude has to be given to my advisor, Prof. Chao Zhou, for giving me this chance to get involved in this project. I was able to extend my knowledge from books to hand-on experiences. As a professor he works even harder than students, having several meetings a week. However, he is still able to work out a schedule to help and discuss details of projects, which is really impressive in terms of his hard-workingness and efficiency. I am also deeply indebted to Mudabbir Badar for what he has taught me. During the period that I was learning and doing the experiments, he was always there and gave me a lots of help. Whenever I have any questions, he tried his best to make things clear. He is a man of meticulousness and cautiousness. I learned a lot from the way that he did things; he is never satisfied with the results. He has to try the same process several times so that he has iron-clad confidence to accept the values that he measured. There are not enough thanks to him for what he has made for me. Lastly, my family is the biggest support for my life throughout the master's program, spiritually and financially. They respect my choice when I decided to study abroad for my Master's and give me full support for it, without any hesitation. Were it not for their selfless support I wouldn't be able to hold on to it and go through the hard time here and there. Again, there is no adequate word to describe their love and help to me.

Table of Contents

List of Figures

List of Tables

Abstract

OCT has been taking an important role in medical imaging. Firstly used as a time domain model, it's somewhat limited by its speed. However, speed is significantly improved after the introduction of Fourier Domain OCT. Since this imaging method is commonly used in ophthalmology, it requires higher speed to reduce motion artifacts. It's also known that higher sensitivity is a favorable factor in OCT too. Resolution also takes an unnegligible role here. With better resolution we can delve into tissues with more clear images, which leaves us more information available for analysis. With all that being said, it's not hard to imagine how many efforts have been put into it to achieve higher speed, sensitivity and resolution. We, as a part of this field, are also striving to achieve this goal. By using integrated photonic chip which has a three layer cascade of 1X2 splitters to split incident light into 8 beams we can not only reduce the complexity of the structure of fiber optics in its prototype but also lower the cost. From [5,6] we know that the speed is proportional to the number of beams, and an imaging speed of 800, 000 A-scans/s was achieved with a sensitivity of 91 dB. In this paper an improved version of Space Division Multiplexing OCT system based on the previous systems was demonstrated with an increase of sensitivity by 6dB, from 91 dB to 97dB.

1. Chapter 1

1.1 Introduction

In light of high demand in clinical uses, more and more techniques, invasive or noninvasive, were developed to meet the demand. By using noninvasive techniques, getting a knowledge of a patient's condition without doing any harm to the patient is achievable. Noninvasive techniques in imaging include ultrasound, optical coherence tomography, and confocal microscopy, just to name a few common ones. Resolution of ultrasound normally falls in the range from 0.1 mm to 1mm depending on the sound wave frequency. One can even obtain up to 15 μm with frequencies at round 100M Hz [1]. However, as the frequency goes higher the penetration will be strongly weakened in tissues, with imaging depth being limited to a few millimeters. Confocal microscopy can achieve as good resolution as up to 1μm, however, it suffers from the same penetration issue because of the optical scattering in biological tissues, with the depth limited to a few hundred micrometers [1]. With the advent of Optical Coherence Tomography, the gap between ultrasound and confocal microscopy can be filled. OCT has the capability of reaching around 1 to 15 μm for resolution while still being able to keep the penetration depth at around 2 millimeters. The high resolution of OCT technique allows us to form a tomographic structure of subjects, such as retina, cornea, and so on [2]. But, this technique also has the same problem in terms of scattering in tissues. When light beam goes deeper into tissues, it will encounter higher scattering and stronger attenuation, which therefore

put a cap on penetration depth. But one can still take advantage of its property to acquire two or three dimensional image for better analysis.

Over the past two decades after its introduction to the world, development of more powerful optical coherence tomography (OCT) systems have been of great interest for many researchers. The commonly available techniques for Optical Coherence Tomography can be generally divided into two groups, one is in Time Domain (TD-OCT), the other in Fourier Domain (FD-OCT), which can be further subgrouped into Spectral Domain (SD-OCT) and Swept Source (SS-OCT) [3]. Optical Coherence Tomography was firstly proposed as a time-domain model, which is built on a system with a moving reference arm for data acquisition, as shown from Figure (1). In the first time domain model one can acquire cross-sectional images but with very poor quality [2,3,4]. The principle of the method is that by employing the property of light coherence, we can obtain information from different layers of samples. By taking advantage of the property of coherence, we are able to bypass the problem that comes from the speed of light. Since speed of light is too fast in terms of sampling frequency of the system, there is no direct way to measure how much light has traveled. Light waves will have interference only when the difference of optical path length between two arms is within coherence length. Information of tissues from corresponding locations can be found by analyzing the interference fringes. OCT is widely used in the fields like biological imaging, medical diagnostic, material inspection and so on. The commercial available products can be found in the use of ophthalmology and optometry, in which we can employ this technique to acquire detailed information from retina, interventional cardiology for diagnosing coronary artery disease and some dermatological purposes.
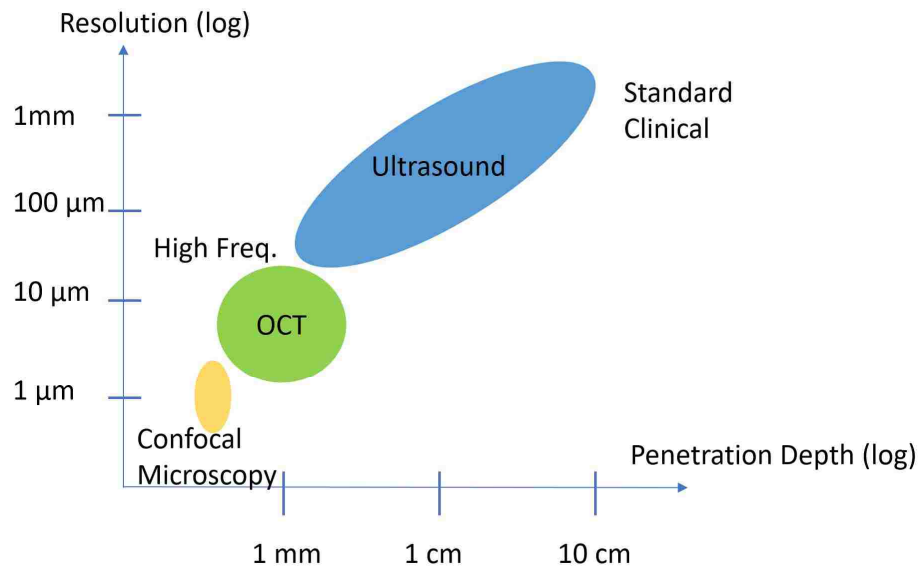
Figure 1 In the graph we can see the role that OCT takes, which fills up the gap between Ultrasound method and Confocal Microscopy.

1.2 Principles

OCT is a system based on interferometry. In certain aspects, the technique used in OCT is somewhat similar to the one used in ultrasound imaging, but instead of using ultrasound waves to acquire echoes (reflections), low coherence property of a broadband light source to measure reflections from samples was employed, in which a Michelson interferometer is used for measurements. From equation (1.8) that the broader the bandwidth, the shorter the coherence length. By using this property, we can thus prevent interferences that bounce several times within sample and therefore deviate away from coherence length. The core idea of OCT systems is that desired signals are acquired when they interfere coherently. Originally, time

3

domain OCT was used for scanning. However, this version was severely affected by its slow acquisition time and its relatively complicated structure for real time imaging. After the development of Fourier Domain OCT, speed and sensitivity are significantly improved compared to TDOCT. Two spectral based optical coherence tomography systems are developed. One is Spectrum Domain Optical Coherence Tomography (SD-OCT) and the other is Swept Source Optical Coherence Tomography (SS-OCT) [3]. SD-OCT uses a broadband light source with a 1-D array CCD to receive signals while SS-OCT employs tunable wavelength light source with a photodetector to acquire data. From the publication by [5], sensitivity has well improved in both spectral domain systems in comparison to TD-OCT. A simplified mechanism of OCT systems is as follows. After a light source emits a source beam, it will be split into two beams by a beamsplitter, with one heading to reference arm and the other to sample arm. Both backreflected beams will be regrouped by the beamsplitter and collected by a detector. From [3], we know that backreflected beams can be expressed as follows:

$$E_R = E_{R0} \exp(i(2\, k_R\, l_R - \omega\, t)),$$

(1.1)

$$E_S = E_{S0} \exp(i(2\, k_S\, l_S - \omega\, t)),$$

(1.2)

Here E_{R0} and E_{S0} represent initial amplitude of the two beams; k_R and k_S the constants of propagation in both beams; l_R and l_S the path length measured from beamsplitter to backreflection surfaces. A factor 2 was put in front of k due to the fact that same route was taken twice in each arm. Note that the recombined electric field E can be shown as

4

$$E = E_R + E_S.$$

And photocurrent i(t) at the detector is

$$i(t) = \frac{\eta e}{h\nu} \frac{<|E_s + E_t|^2>}{2Z_0}$$

(1.3)

η stands for efficiency of the quantum in the detector, e for charge of electron, $h\nu$ for photon energy, Z_0 for the intrinsic impedance in free space. i(t) is averaged over the response time of the detection system. For simplicity, the following form was taken to express short-time-averaged light intensity.

$$I(t) = |E_R + E_S|^2$$

Replacing equation (1.1) and (1.2) into the equation above gives us

$$I(t) = E_{R0}^2 + E_{S0}^2 + 2 E_{R0} E_{S0} \cos(2 k_S l_S - 2 k_R l_R).$$

(1.4)

The cosine term comes from the interference between two light beams and contains the information that is useful. Here difference of the phase between two beams is defined as

$$\Delta\phi = 2 k_S l_S - 2 k_R l_R.$$

(1.5)

When $\Delta\phi$ changes the value of the cosine term in equation (1.4) will change like an alternating current that has interference fringes, which is why the recorded I is also called interferogram. Making $k_R = k_S = k = \frac{2\pi n}{\lambda_0}$, in which n stands for refractive index and λ_0 describes the optical wavelength in vacuum, helps simplify the case and (1.5) becomes

5

$$\Delta\phi = 2k(l_S - l_R) = 2\pi \frac{2n\Delta l}{\lambda_0},$$

<div align="right">(1.6)</div>

where the term in the bracket is defined as arm-length difference between these two arms.

$$\Delta l = l_S - l_R$$

<div align="right">(1.7)</div>

A round-trip of arm-length difference makes path length difference equal to $2\Delta l$. Lastly, difference of optical path-length between two arms can be defined as $2n\Delta l$. Note that from the equation (9.15) [8] it's known the that definition of coherence length is

$$l_C = \frac{4ln2}{\pi} \frac{\lambda_0^2}{\Delta\lambda},$$

<div align="right">(1.8)</div>

where λ_0 is the center wavelength of the light source and $\Delta\lambda$ is the FWHM bandwidth in wavelength. Equation (1.8) shows that the broader the bandwidth of the light is, the shorter the coherence length becomes.

1.2.1 TD-OCT

In order to collect signals from different depths, TD-OCT does it by moving the reference arm. Due to the fact that a broadband light source was used in the system, only backscattering signals that are within coherence length will interfere with light beams from reference arm. And it's due to the same reason that in this system it's necessary to keep moving the reference arm so that signals can be collected from different depth, which leads to longer acquisition time. In Figure (2) there are three peaks, each of which represents a corresponding location in the tissue, in the intensity diagram. These three locations are measured during the shifting of the reference arm, and an A-scan can be obtained after the process is completed along the z direction. All the

interference signals are recorded by a photodectector. TD-OCT still has a few advantages, such as elimination of coherent noise and symmetric images, over FD-OCT even though it is relatively slower and unstable, the latter of which originates from the fact that reference arm has to be kept moving to acquire information from different locations.
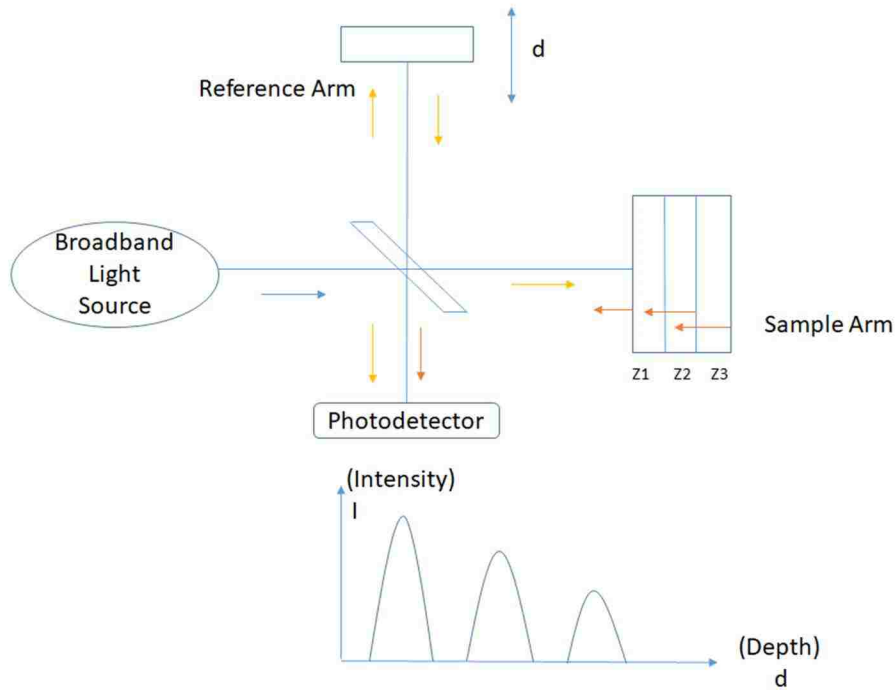

Figure 2 Beams from the source get splitted by the beam-splitter. At specific position d(x) of the reference arm, backreflected beam from a certain location will only interfere with the reference arm beam when the optical path length difference falls within coherence length.

1.2.2 FD-OCT

Instead of measuring locations by shifting the reference arm, information of different locations is coded in the frequency. Hence, take A-scan for example, TD-OCT requires individual scanning of each location to complete a full A-scan, however, FD-OCT can collect information from different locations just by one scanning on a spot. It's not hard to see that FD-OCT can largely reduce acquisition time just by doing Fourier Transformation on signals. From [15], the intensity at the output of the interferometer can be described as:

$$I(\tau) = I_0 \left(a_r + \sum_n a_n + 2 \sum_{m \neq n} \sqrt{a_n a_m} \, \text{Re}\{ \gamma_{ss}(\tau_{nm})\} + 2 \sum_n \sqrt{a_r a_n} \, \text{Re}\{ \gamma(\tau_n)\} \right)$$

(1.9)

where coefficient a_r and a_n are coefficients of attenuation of light in reference arm and sample arm respectively, $\gamma(\tau)$ the complex degree of the coherence. The third term inside the bracket of equation (1.9) is the mutual interference between the light waves backreflected within a sample. By Fourier Transforming equation (1.9), the light spectrum can be expressed as:

$$S_{total}(\omega) = S(\omega) \left[\left(a_r + \sum_n a_n + 2 \sum_{m \neq n} \sqrt{a_n a_m} \, \cos(\tau_{nm}\omega) + 2 \sum_n \sqrt{a_r a_n} \cos(\tau_n \omega) \right] \right.$$

(1.10)

To obtain the reconstruction of the axial structure of the sample, application of inverse Fourier Transformation was used. Equation (1.10) becomes

$$\hat{\gamma}(\tau) = \left(a_r + \sum_n a_n \right) \Gamma(\tau) + \sum_{m \neq n} \sqrt{a_n a_m} \left(\Gamma(\tau) \otimes \delta(\tau \pm \tau_{nm})\right) + \sum_n \sqrt{a_r a_n} \left(\Gamma(\tau) \otimes \right.$$

$$\delta(\tau \pm \tau_n))$$

(1.11)

With only the signals from the fourth term being interested in, the first three terms are considered as coherence noise, which comes from reflections within measurement instrument

or mutual interference between light waves backreflected within an object. The simplest way to get rid of coherence noise is to subtract measured signals when there is not any object on the sample arm. However, coherence noise originating from the sample is harder to be taken away. Another problem from FD-OCT system is that we will have two symmetrical images, which roots from the fact that $S_{total}(\omega)$ is a real-valued function[4], when the image of the object is reconstructed, in which case it makes it harder to have a reliable analysis of the observed image. Unlike TD-OCT, which measures only some of the backreflections at any one time, all the backscatterers on the A-scan from the sample are measured at the same time and thus speed is largely improved in FD-OCT systems. To build FD-OCT systems, there are two common ways to do it. The first one is Spectral Domain Optical Coherence Tomography, Figure (3), in which it uses a spectrometer that is equipped with a high-speed line scan detector to collect signals from the interferometer. Interference signals will first go through diffraction grating to be split into different wavelengths, and individual wavelength will be received at corresponding camera. The second one is Swept Source Optical Coherence Tomography, Figure (4), in which the light source sweeps through the whole bandwidth in accordance with time and selects only certain wavelength. Interference signals are collected by a photodiode. Both resolution of SD-OCT and SS-OCT contingent on the bandwidth of the light source. Acquisition time in SD-OCT, however, relies on the exposure time of CCD camera, whereas in SS-OCT acquisition time depends on the sweeping rate.
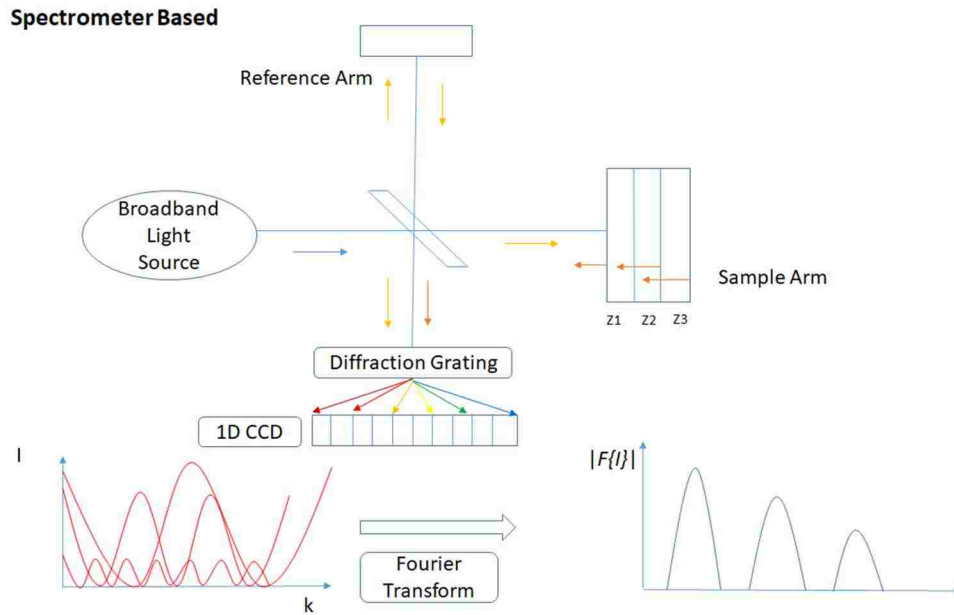
Figure 3 shows a simplified schematic of SD-OCT system, where we can see the interference signals go through diffraction grating before they reach 1D CCD camera. After signals are received they will be fourier transformed to retrieve information from the sample
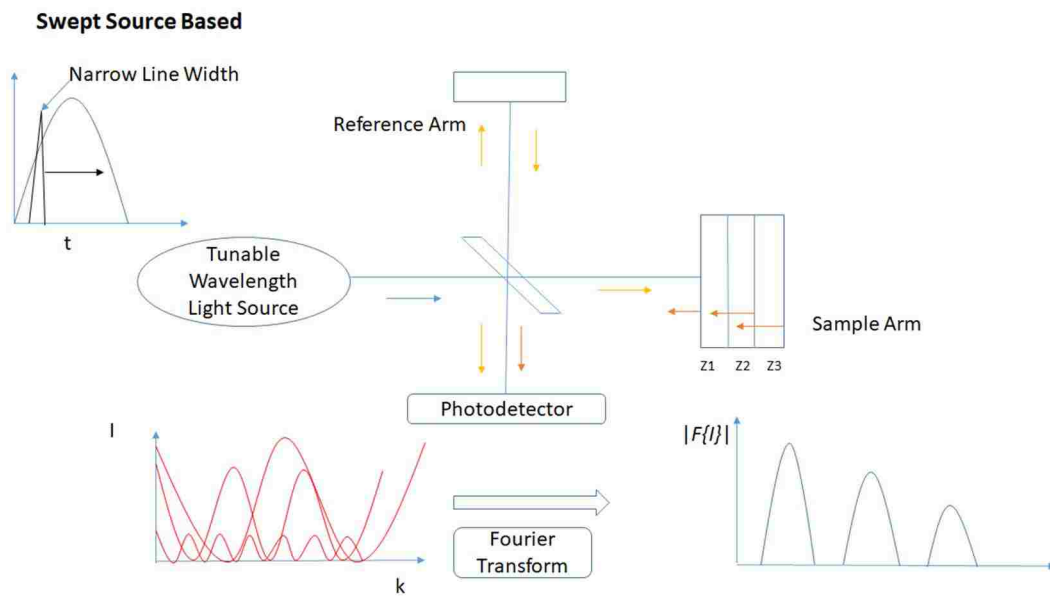

Figure 4 shows the schematic of SS-OCT system, in which a narrow line width wavelength is selected at each sweeping and since it has narrower bandwidth it can acquire more interference signals from deeper tissues.

1.2.3 Comparison of sensitivity

Sensitivity of OCT systems are of great concern of researchers, the higher the sensitivity, the better the image contrast one can have. It's not until researches in [9,10] that clearly showed the performance and advantages of Fourier Domain OCT over Time Domain OCT. In [9], it's shown that SNR in TD-OCT can be expressed as follows

$$SNR_{TD-OCT} = \frac{\lambda_0^2}{Z_{max}\Delta\lambda_{FWHM}} \frac{\rho P_0 T}{e} \frac{\gamma \gamma R_r R_s}{(R_r+R_s)} \tag{1.12}$$

where Z_{max} is the optical length in correspondence to the maximum axial imaging range; P_0 average power entering the interferometer; R_r and R_s for reflectivity coefficient of reference and sample arm respectively. From the same paper it's also known that sensitivity in FD-OCT and TD-OCT can be related as

$$SNR_{FD-OCT} = \frac{2ln2}{\pi} \cdot \frac{Z_{max}}{\Delta z} \cdot SNR_{TD-OCT} \tag{1.13}$$

Typically the ratio of axial imaging range to the axial resolution is higher than 1 in tissue imaging using OCT, reaching values to the order of ten to the power three. By simply plugging the physical ratio to (1.13) it's seen that a theoretically 30 dB improvement of sensitivity in FD-OCT over TD-OCT. Note that the improvement of axial resolution is a benefit for FD-OCT. However, one thing has to be mentioned, better sensitivity of FD-OCT systems is based on certain well-defined conditions, in which we can have the ratio much bigger than 1. In the experiment results from [9], sensitivity of 121 dB was measured, which is in accordance with the expected value 126 dB calculated from equation (10), whereas sensitivity predicted by equation (9) is 107 dB. In this experimental setting it's observed either experimental or

theoretical value is significantly better than the value one can have in TD-OCT system.

2. Chapter 2

2.1 Method

2.1.1 Space Division Multiplexing Optical Coherence Tomography

Achieving higher imaging speed not only helps us expand the applications of OCT into in vivo fields but also reduces the problems that originate from motion artifacts. The first TD-OCT only has an imaging speed of 2 A-scans/s [3]. The scanning speed of 4000 A-scans/s was achieved by Rollins et al [11] in 1998. It's not until the publication of [12] that showed a prominent leap from a few thousands to 15,000 A-scans/s. However, advancement in new wavelength-tunable lasers has even made another milestone for imaging speed, reaching as fast as several million A-scans/s [13,14]. Currently high speed versions of optical coherence tomography systems are mainly built on SS-OCT systems. But unfortunately there is also a trade-off of having faster wavelength-tunable lasers. The faster the lasers are, the worse the performance might be due to severe roll-off in sensitivity and restrained axial resolution because it's harder to keep broad wavelength ranges when imaging speed goes high [15, 16].

In order to gain the most out of imaging speed while not losing its sensitivity and resolution, parallel imaging was supposed. Using several beams to image different parts of the sample at once helps achieve high imaging speed. One way of doing it is by employing multiple sources to image different locations of the sample. Another way of parallel imaging is to utilize interleaved OCT (iOCT) to improve imaging speed [17,18,19,20]. However, both of the techniques suffer from either high cost and complexity of the system or cross-talk between

channels due to short separation between each beam, respectively. A method was proposed in [7] to improve imaging speed by using a different parallel imaging method called Space Division Multiplexing. Multiple channels with various optical delays were made by splitting a single sample arm beam and these split beams were employed to acquire images of different parts

on the sample, shown in Figure 5. It's obvious that imaging speed will increase as the number of beams increases. In [7] eight channels were used and an imaging speed of 800,000 A-scans/s was achieved with a VCSEL laser running at 100k Hz. The prototype of this method proposed in [7] requires a huge amount of time and work to manually adjust the setup, including assembling fiber components and controlling individual optical delays of each channel. Due to this reason, it's a great barrier ahead to popularize and manufacture this system in a large scale. Therefore, the group in Zhou's lab [6] proposed an idea of using an integrated photonic chip to accomplish this job. It's also known that using integrated chip can not only lower the expense and size but also enhance the stability of the entire system [21]. In their demonstration, three layers of 1 X 2 splitters were incorporated into the chip to ramify a single incident beam into eight beams with an optical delay of around 2.5 mm between each channel to create multiplexed interference signals. It showed the integrated chip can work as well as the first lab prototype with the speed reaching 800,000 A-scans/s and the sensitivity being around 91 dB. To test the performance, three dimensional images of the volume of 700 X 1200 A-scans/s of ex vivo porcine eye and an in vivo human finger print with an area of 18.0 X 14.3 mm^2 were acquired in ~1 seconds.
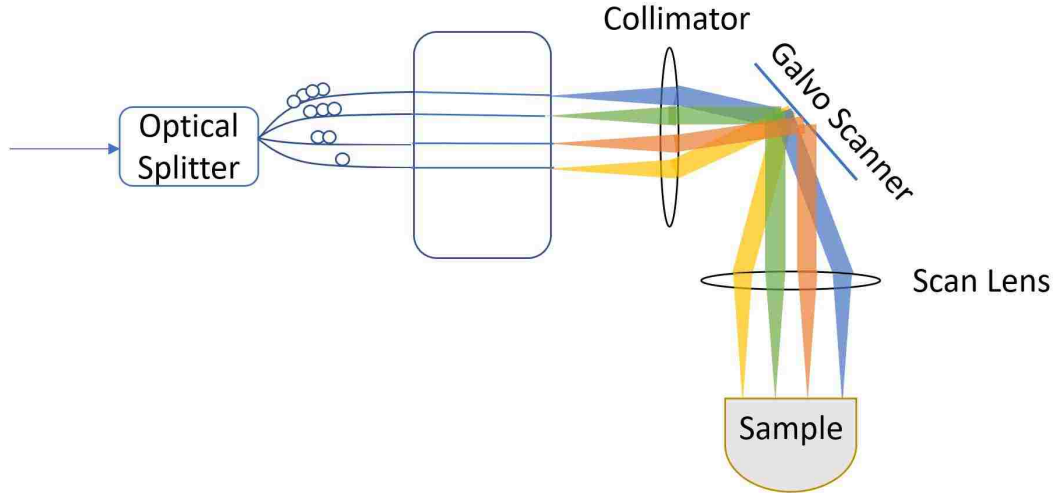
Figure 5 shows how one incident beam was split into multiple beams. For simplicity only four beams were shown.

2.1.2 Integrated photonic chip

To reduce the hassle and facilitate the process of setup of the SDM-OCT system, an idea of utilizing integrated photonic chip was proposed by [6]. Results from the first chip was not much different from the first lab setup, in which the sensitivity of chip-based system is around 92 dB while that of the first nonchip-based system was around 94 dB. Performance of the proposed system was proven not to be affected by using integrated chip. However, the sensitivity of the first chip-based system was only 92 dB and knowing that 6 dB was lost to the splitting loss an improved design of the optical path of backreflected beams that can theoretically help us reduce 6 dB loss was came up with, which means it's achievable to have 97 dB in sensitivity.

2.1.2.1 First Generation Chip

Three layers of 1X2 splitters was used in the first generation chip. A single incident light beam was split into 2 beams after the first layer. Completing the process through next two layers lead to the formation of eight beams with the distance between each beam being 25 mm, as seen from Figure 5. (B). A commercially available VCSEL wavelength tunable laser (SL1310, Thorlabs Inc., USA) was utilized, followed by a booster optical amplifier (BOA, BOA1130s, Thorlabs Inc., USA) to amplify the power of the output of the laser source from around $27\ mW$ to around $100\ mW$. The amplified light went through a 97/3 optical coupler which transmitted 3 percent of the light to a customized Mach-Zender interferometer (MZI) with an optical delay of 38.7mm being used for phase calibration and the rest of the power of the light was kept for imaging. The imaging light further went through a 95/5 optical coupler to have 5 percent of the light used in the reference arm and the other 95 percent for sample arm. The incident beams on sample arm were then combined to the integrated photonic chip before going through a circulator (AC Photonics, Inc) and a polarization controller. Collimation of all beams from the output of the chip was made, with a telescope setup which has a 30mm lens and 50mm lens to enlarge the beam size. Wide-field volumetric imaging was achieved using a large scanning lens (LSM05, Thorlabs Inc., USA) mounted on the sample arm after the XY galvanometer mirrors. Incident power on each beam shared same intensity of around 3 mW. Signals that are reflected back from both arms were directed to a 50/50 optical coupler by a circulator. Interference signals of OCT and MZI were detected by dual-balanced detectors

16

(PDB480C-AC, 1.6 Hz, Thorlabs Inc.) and the outputs were obtained by a dual-channel high-speed acquisition card at the same time (ATS 9373, Alazar Technologies Inc.) with a sample rate of 1.5GS/s. In order to avoid aliasing, sampling rate was kept at least twice as much as the max frequency of the fringe to comply with Nyquist theorem. The setup of the system is described in the schematic. When the light is reflected back, it goes through three layers of 1X2 splitters, each of which contributes to 3dB loss. Therefore as suggested by [8], an overall 15 dB loss, including transmission and splitting loss, as compared to the calculated shot-noise-limited sensitivity was expected. Figure 5. shows the illustration of the setup based on the first generation chip. The spacing between beams ,layout and size of the chip were also available in inserts (B), (C) and (D). Note that 0.25 mm was measured for the spacing between beams. In insert (E) the measurement of roll-off of the central beam based on the first generation chip was shown in logarithmic scale, in which a 2 dB roll-off at 27 μm was observed. (F) showed the transverse resolution of this chip was 20 μm using USAF target.
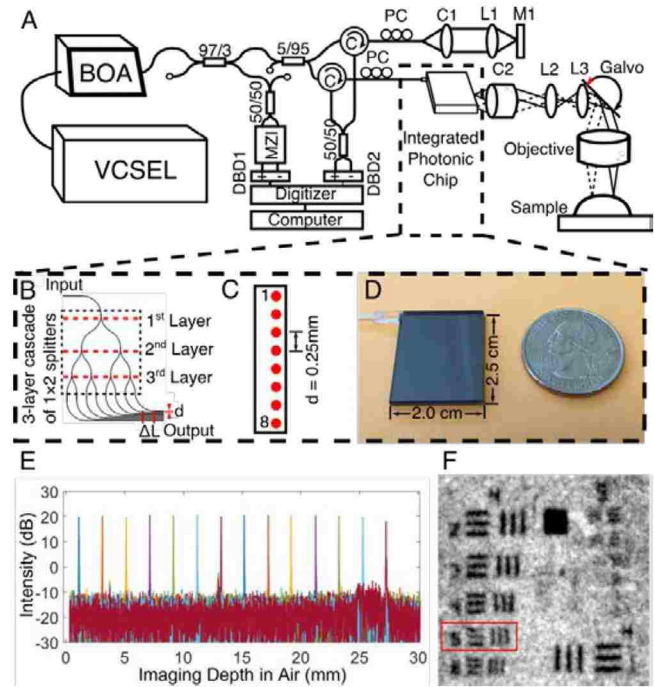
Figure 6 (A) Illustration of the setup of the chip-based system. (B) Layout of the first generation chip showed three layers of 1X2 splitter. (C) An enlarged demonstration for the spacing between beams. (D) Comparison between the size of the chip and an US quarter. (E) A 2 dB roll-off of the systems was measured at 27 μm with imaging depth being 31 μm in air. (F)An USAF test was used to measure transverse resolution. 20 μm of transverse resolution was measured and stripes were still differentiable in Group 4, Element 5.(C for Circulator; C1, C2 for collimator; DBD1, DBD2 for dual balanced detectors; L1, L2, L3 for lenses; M1 for mirror; PC for polarization controller.) (Cited from Yongyang Huang's paper [6])

2.1.2.2   Second Generation Chip

To avoid extra 6 dB loss when light was backreflected to the three layers of splitter, beams were directed, at the third layer of the sample arm, to the reference arm for interference. Figure 6 shows a simplified layout of the second generation chip. Notice that in this chip reference arm was also integrated instead of being operated outside the chip, as can been seen from Figure 5. The whole setup for the second generation chip wasn't changed much. A similar

structure can be found from the first chip-based setup. However, to create a better result a few modifications were added to the new setup. Same as in the first setup, a VCSEL wavelength-tunable laser (SL1310V1, Thorlabs Inc., USA) with central wavelength set at 1310 μm was used. After the laser immediately follows a booster optical amplifier (BOA, BOA1130s, Thorlabs Inc., USA). Then the light went through a 95/5 optical coupler instead of 97/3 one, using 5 percent of the power for phase calibration and 95% of it for imaging. The remainder was further split by a 90/10 optical coupler where 10 percent of the power was used for reference arm and the rest for sample arm. Light going to reference arm was collimated and focused using a collimator and lens respectively before reaching a polarization controller. A circulator and a polarization controller were used for the power going to the sample arm. Signals obtained after interference were divided into two bundles with four beams in each. Each bundle was then combined by a multimode fiber combiner before they were collected by a multimode ballistic photodetector.

Reference   **Sample**

1st Generation

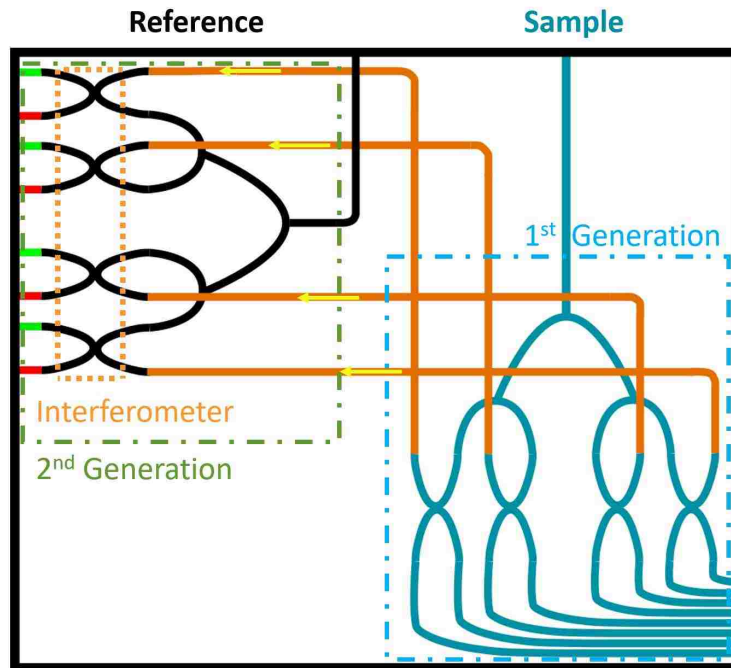Interferometer

2nd Generation

Figure 7 shows the configuration of the second generation chip. The difference of the chip from the first generation is mainly on the redesign of the reference arm. In the first generation the reference arm was built outside the chip, while in the new one it's combined into the chip with the interferometer. The orange lines are the backreflected beams routed from the third layer of splitter of the sample arm. They then interfere with the reference arm.
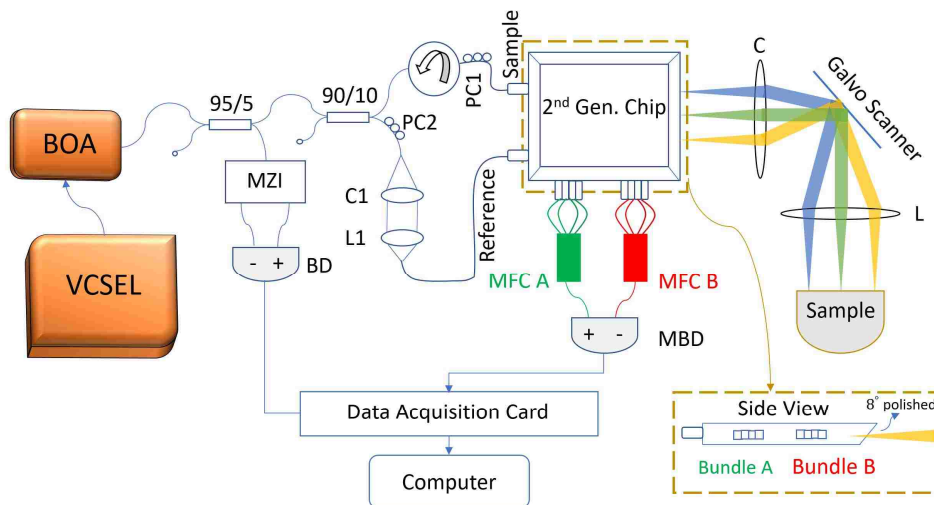

Figure 8 shows a simplified setup based on second generation chip. Main differences of the new setup were indicated below. Two optical couplers were changed to 95/5 and 90/10 respectively. Reference arm was integrated into the second generation chip. Two multimode fiber combiners were used and the original balanced detector was changed to multimode balanced detector. The little box on the bottom left shows the side view of the chip. It's seen that the façade that emits beams was 8 degree polished.

20

3. Chapter 3

3.1 Experiments and Results

OCT system is a very sensitive setup, therefore, correct alignment of the system plays a key role of whether a good result can be obtained or not. Several trials have to be made until a satisfying alignment is acquired. Furthermore, mounts with different degrees of freedom are needed for fine tuning. During the tests of the second generation chip, self interference from within the chip was observed. In order to solve this problem, the façade of the chip was polished by 8 degree to reduce the self interference, shown in Figure 7. The general setup of the OCT imaging system isn't changed much, with main difference being a new design of the chip. The target of the second generation chip is to enhance the performance of the system by bypassing the first and second layer splitter so that the sensitivity can be increased by 6 dB. As expected, power on the sample for both chips doesn't change and same applies to the resolution for both. Sensitivity of the high power beam, however, did meet the expectation by increasing another 6 dB from 92 dB. One thing has to be noted here, the power of the eight beams in second generation chip is not uniform, which doesn't exist for the first generation chip. This non-uniformity leads to a problem that a high-low pattern was observed. Hence, four of the beams have an output of 1.6 mW while four have 3 mW for the output power. Table (1) shows the comparison of the sample power, resolution and sensitivity of the two chips. It's seen that the sensitivity of the low power beam was 95 dB while that of high power beam was 98 dB. Both of these beams showed an increase of sensitivity by at least 3 dB from 92 dB. The measurement

of the sensitivity was done by placing a mirror on sample arm, and a pinhole was put on top of it to allow only one beam to pass through, in which only the center beams were used for sensitivity measurement. Analyzing measured light power back reflected from the mirror with the help of pre-written code gives the sensitivity.

	Sample power	Resolution	Sensitivity
First Gen Chip	3 mW	11 μm	92 dB
Second Gen Chip (low power beam)	1.6 mW	12 μm	95 dB
Second Gen Chip (high power beam)	3 mW	12 μm	98 dB

Table 1 shows the comparison of the power on the sample, resolution and sensitivity of the chip for both generation. Note that there exists non-uniformity in the second generation chip, so it's divide into two rows for individual comparison.

To test the quality of the image of the second generation chip, imaging was tested on Scotch tape. Figure 8 shows the image using modified chip whereas Figure 9 shows the image using the first prototype chip. For fair comparison of the image quality, image from the same beam was chosen, where 3rd beam was used in this case. Gaps between layers were easy to differentiate and the axial resolution was improved in the modified chip, where spacing between deep layers of Scotch tape were still able to be distinguished. However, referring to Figure 9 immediately shows a blurry image and it's hard to differentiate deeper layers. Two things have to be mentioned, first only 7 beams were tested on imaging for the prototype chip. The eighth beam was left out because of the issue of out of focus. Second, only two beams being used in the modified chip was due to the fact that four photodetectors used to combine

beams introduced extra 6 dB loss, which exactly balanced out the expected improvement of the
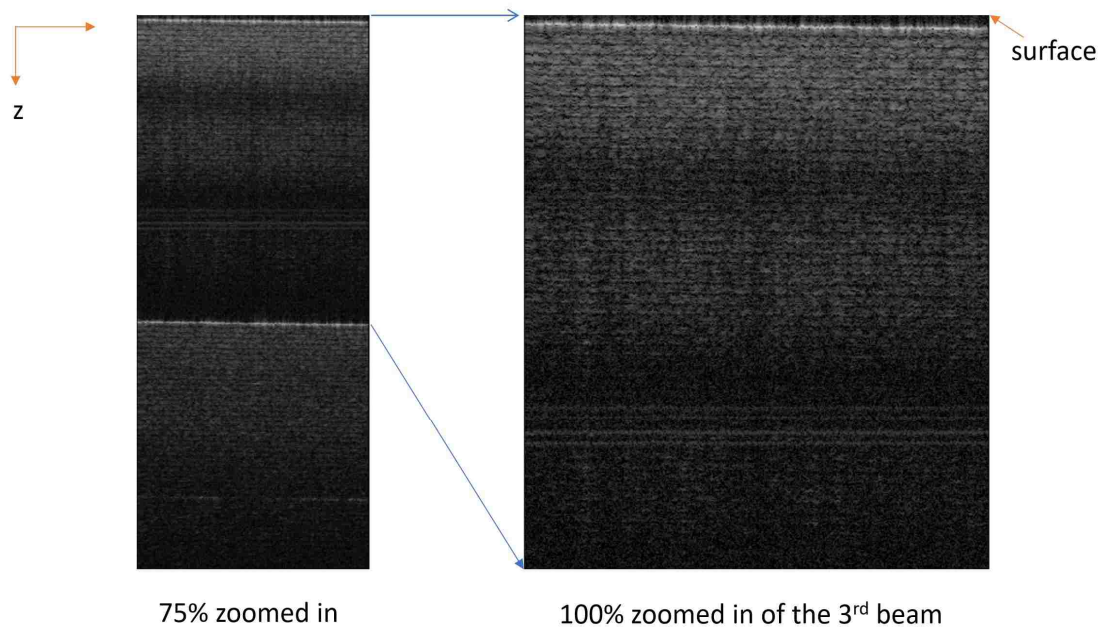
sensitivity of the chip.

75% zoomed in   100% zoomed in of the 3rd beam

Figure 9 shows the image using only 3rd beam and 4th beam. In the enlarged picture of the 3rd beam layers of the scotch tape are easy to be differentiated and deep layers are still clear and observable.

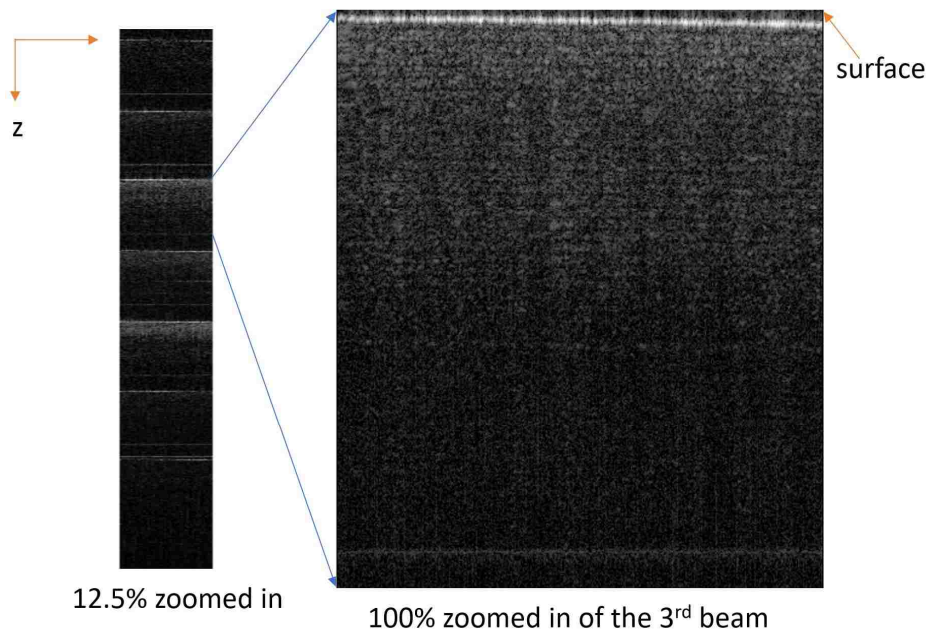12.5% zoomed in   100% zoomed in of the 3rd beam

Figure 10 shows the image of the scotch tape, and 3rd beam was chosen for fair comparison. Layers of the tape

were barely seen and it's hard to differentiate each layers. Resolution becomes worse when it goes deeper.

4. Chapter 4

4.1 Discussion

An improved design of the chip was demonstrated. The new design of the chip showed an incorporation of both reference arm and sample arm into the chip. Improvement of the sensitivity by 6 dB was also shown. However, several problems have to be mentioned here. First, self-interference was observed during the experiments. Several trials of realigning the setup were made but failed. In order to reduce the self-interference, chip was sent to be 8 degree polished. However, lack of adequate devices to check the precision of the polishing lead to the uncertainty of whether the chip was perfectly polished. It can only be told by reading the figures on computer to see if self-interference was reduced, which means several polishings may be considered. Second, non-uniformity of the power of eight beams was observed in the second generation chip, which was not a problem in the first prototype chip. Beams should have shared same amount of power, which in this case should have been 3 mW for each beam. A high-low pattern was seen in the newly-designed chip. 3 mW was measured in high power beams, while 1.6 mW was measured in low power beams. Inconsistence of the power of the eight beams also made the contribution to the difference of the sensitivity between the high power beams and low power beams. Sensitivity of high power beams was observed to be 6 dB more than the first prototype chip whereas that of low power beams was only 3 dB higher than the first generation

chip. Overall, this issue contributed a total of 3 dB loss to the system. Third, imaging the Scotch tape using only two beams showed an improvement in both sensitivity and image quality. However, scanning using eight beams wasn't successful in creating better sensitivity and image quality. One suspicion that this problem may be attributed to the insertion loss from the photodetectors, which combined two beams per one, was considered. The total loss from four detectors combined amounted to 6 dB, which exactly balanced out our expected gain from the new chip. To test the possibility, a new multimode fiber combiner that can combine multiple beams at once was ordered. Experiments with this new detector can not be finished before the submission of the thesis. With all the aforementioned issues fixed, the sensitivity of the chip can be further enhanced by at least another 3 dB.

5. Chapter 5

5.1 Conclusion

Performance of the newly designed chip was proved to be better than that of the old version. An increase of 6 dB in sensitivity was demonstrated. Sensitivity can be further improved if the problem of non-uniformity and extra loss from fiber combiner can be solved. Image quality based on the new version of the chip showed clearer layers. Also the axial resolution was enhanced because layers were still differentiable when one goes deeper. To make a more accurate comparison between these two generations, imaging scanning has to be done with eight beams combined. A multimode fiber combiner that can group these eight beams is needed for further tests. The group is working on testing the performance of the modified chip with a multimode fiber combiner. More experiments are needed for further improving the performance of the chip.

6. References

[1]   https://zmpbmt.meduniwien.ac.at/wissenschaft-forschung/optical-imaging/morphological-imaging/

[2]   E. A. Swanson, J. A. Izatt, M. R. Hee, D. Huang, C. P. Lin, J. S. Schuman, C. A. Puliafito, and J. G. Fujimoto, "In vivo retinal imaging by optical coherence tomography," Opt. Lett. 18, 1864–1866 (1993).

[3]   D. Huang, E. A. Swanson, C. P. Lin, J. S. Schuman, W. G. Stinson, W. Chang, M. R. Hee, T. Flotte, K. Gregory, C. A. Puliafito, and J. G. Fujimoto, "Optical coherence tomography," Science 254, 1178–1181 (1991).

[4]   M. R. Hee, C. A. Puliafito, C. Wong, J. S. Duker, E. Reichel, J. S. Schuman, E. A. Swanson, and J. G. Fujimoto, "Optical coherence tomography of macular holes," Ophthalmology annual 102, 748–756 (1995).

[5]   L. V. Wang and H. Wu, Biomedical Optics (Wiley, 2007).

[6]   Yongyang Huang, Mudabbir Badar, Arthur Nitkowski, Aaron Weinroth, Nelson Tansu, and Chao Zhou , "Wide-field high-speed space-division multiplexing optical coherence tomography using an integrated photonic device", Biomedical Optics Express, Vol. 8, Issue 8, pp. 3856-3867 (2017)

[7]   Chao Zhou, Aneesh Alex, Janarthanan Rasakanthan, and Yutao Ma, "Space-division multiplexing optical coherence tomography", Opt. Express 21(16) 19219-19227

(2013)

[8]   M. Wojtkowski, A. Kowalczyk, R. Leitgeb, and A. F. Fercher, "Full range complex spectral optical coherence tomography technique in eye imaging," Opt. Lett. 27, 1415–1417 (2002).

[9]   Michael A. Choma, Marinko V. Sarunic, Changhuei Yang, Joseph A. Izatt,"Sensitivity advantage of swept source and Fourier domain optical coherence tomography", Optics Express, Vol. 11, Issue 18, pp. 2183-2189 (2003)

[10]   R. Leitgeb, C. K. Hitzenberger, and A. F. Fercher , "Performance of fourier domain vs. time domain optical coherence tomography ", Optics Express, Vol. 11, Issue 8, pp. 889-894 (2003)

[11]   A. M. Rollins, M. D. Kulkarni, S. Yazdanfar, R. Ung-arunyawee, and J. A. Izatt, "In vivo video rate optical coherence tomography," Opt. Express 3, 219–229 (1998).

[12]   M. Wojtkowski, T. Bajraszewski, P. Targowski, and A. Kowalczyk, "Real-time in vivo imaging by high-speed spectral optical coherence tomography," Opt. Lett. 28, 1745–1747 (2003)

[13]   W. Wieser, B. R. Biedermann, T. Klein, C. M. Eigenwillig, and R. Huber, "Multi-megahertz OCT: High quality 3D imaging at 20 million A-scans and 4.5 GVoxels per second," Opt. Express 18(14), 14685–14704 (2010).

[14]   I. Grulkowski, J. J. Liu, B. Potsaid, V. Jayaraman, C. D. Lu, J. Jiang, A. E. Cable, J. S. Duker, and J. G. Fujimoto, "Retinal, anterior segment and full eye imaging using ultrahigh speed swept source OCT with verticalcavity surface emitting lasers," Biomed. Opt. Express 3(11), 2733–2751 (2012).

[15]   M. Wojtkowski, "High-speed optical coherence tomography: basics and applications," Appl. Opt. 49(16), D30– D61 (2010).

[16]   T. Klein and R. Huber, "High-speed OCT light sources and systems [Invited]," Biomed. Opt. Express 8(2), 828– 859 (2017).

[17]   H. Y. Lee, H. Sudkamp, T. Marvdashti, and A. K. Ellerbee, "Interleaved optical coherence tomography," Opt. Express 21(22), 26542–26556 (2013).

[18]   H. Y. Lee, T. Marvdashti, L. Duan, S. A. Khan, and A. K. Ellerbee, "Scalable multiplexing for parallel imaging with interleaved optical coherence tomography," Biomed. Opt. Express 5(9), 3192–3203 (2014).

[19]   L. Duan, H. Y. Lee, G. Lee, M. Agrawal, G. T. Smith, and A. K. Ellerbee, "Single-shot speckle noise reduction by interleaved optical coherence tomography," J. Biomed. Opt. 19(12), 120501 (2014).

[20]   L. Duan, T. Marvdashti, and A. K. Ellerbee, "Polarization-sensitive interleaved optical coherence tomography," Opt. Express 23(10), 13693–13703 (2015).

[21]   G. Yurtsever, B. Považay, A. Alex, B. Zabihian, W. Drexler, and R. Baets, "Photonic integrated Mach-Zehnder interferometer with an on-chip reference arm for optical coherence tomography," Biomed. Opt. Express 5(4), 1050–1061 (2014).

Vitae

Guo-Jhe Syu was born on February 6th, 1991 to Wu-Hsiung Hsu and Chen-Li Chen. After finishing his bachelor's degree of Electrical Engineering in National Changhua University of Education, Taiwan, he gapped two years to work in a machine repairing shop to gain some experience while preparing for his GRE and TOEFL exams at the same time. In 2016 he got the admission from Lehigh for Master's program in Electrical and Computer Engineering. At the beginning of the program, he had already made his mind that he was going to do a thesis for his Master's degree. Not knowing which topic to do and being kind of lost, he had quite a few discussions with his advisor, Prof. Chao Zhou, who gave him a lot of useful advices and help. Under his advisors' guidance, he was able to learn some skills he hadn't had a chance to know and to finish his master's thesis. After graduation he plans to work in Taiwan in the same machine repairing shop, trying to apply some skills and techniques he learned to his future work and help facilitate processes in the company.